



Research Article

Design and dynamics modeling of a hybrid drive bionic robotic fish

Haoyu Huang, Shuai Xian, Chengye Xiong, Weihua Li, Yong Zhong*

Shien-Ming Wu School of Intelligent Engineering, South China University of Technology, Guangzhou 510641, China

ARTICLE INFO

Article history:

Received 17 February 2025

Revised 18 May 2025

Accepted 9 June 2025

Available online 25 June 2025

Keywords:

Robotic fish, Hybrid drive

Dynamics model

Swimming performance

ABSTRACT

While recent advancements in hybrid propulsion systems for bionic robotic fish—combining biomimetic mechanisms with classical vector thrusters—demonstrate enhanced locomotion capabilities and application potential, challenges remain in modeling the coupled dynamics of heterogeneous propulsion mechanisms. This paper presents a hybrid-drive robotic fish architecture that synergistically integrates pectoral-fin-mounted propellers with a caudal-fin-based propulsion system. A three-dimensional dynamical model is developed to characterize the coupled interactions between the dual propulsion modes, incorporating a hydrodynamic computation framework that accounts for propeller wake effects on caudal fin performance. Systematic experimental validation confirms the model's fidelity through quantitative analysis of swimming performance metrics, including cruising speed, turning radius, and trajectory tracking. The results show that the proposed hybrid propulsion strategy can effectively improve the swimming performance of the robotic fish, and the model can effectively predict the motions such as speed, turning diameter, and trajectory of the robotic fish, which provides a new idea for the development of bionic robotic fish.

© 2025 The Author(s). Published by Elsevier B.V. on behalf of Shandong University. This is an open access article under the CC BY license (<http://creativecommons.org/licenses/by/4.0/>).

1. Introduction

Bionic robotic fish represents a novel autonomous underwater vehicle with significant potential applications in the domains of marine resource survey, fishery monitoring and military operations [1–6]. In comparison with conventional autonomous underwater vehicles (AUVs), the bionic robotic fish is distinguished by its superior maneuverability, minimal ambient noise and reduced energy consumption [7–9]. These characteristics enable more flexible and stealthy missions in ocean exploration, ecological monitoring and military reconnaissance. Enhancing the mobility and three-dimensional movement capabilities of robotic fish can increase their stability in complex underwater environments and their adaptability to multidimensional tasks, thus expanding the range and success rate of practical applications. In the present stage of research, robotic fish that achieve three-dimensional movement through bionic methods, such as bionic pectoral fins and internal buoyancy adjustment systems, exhibit deficiencies including slow response and low anti-interference ability, which fall short of the performance standards of real fish [10]. Propellers possess a broad spectrum of applications in the domain of underwater robotics due to their notable strengths, such as high output power and robust anti-interference capabilities. Consequently, a hybrid propulsion system that integrates multiple propulsion modes through meticulously designed strategies holds promise in enhancing the maneuverability and adaptability of robotic fish.

Currently, in the research of bionic robotic fish, the propulsion mechanisms can be categorized into two main modes: mid-and/or paired fin mode (MPF mode) and body and/or caudal fin mode (BCF mode) [11,12]. The current propulsion mechanisms of these devices primarily encompass single joint/multi-joint mechanisms, wire-driven mechanisms, and smart material drives [13]. Zhong et al. designed a robotic fish equipped with a wire-driven mechanism that emulates the skeletal structure and muscle arrangement of real fish [14–17]. They achieved the dynamic swimming of the bionic robotic fish by integrating an active steel wire-driven body with a flexible submissive caudal fin. Cen et al. proposed a bionic robotic fish based on a flexible two-chip macrofibre composite (MFC) piezoelectric laminate [18]. Andrew et al. developed a bionic robotic fish driven by a series of fluid-elastomer brakes [19]. The fluid-driven system provides the robotic fish with rapid acceleration and continuum body motion, thereby enabling a fast escape response. Chen et al. designed a magnetic-driven miniature robotic fish to enhance the motion amplitude by driving the caudal swing through the spiral tube translation [20]. However, there is a problem of magnetic field interference. Liu's hydraulic double-jointed soft-bodied robotic fish realizes the bionic flexible swing, but the system is complicated and lacks three-dimensional motion [21]. Concurrently, a substantial body of research has centered on the development of robotic fish capable of spatial locomotion. Chen et al. developed a miniature three-dimensional bionic robotic fish with depth control, capable of rapid ascent and descent via water electrolysis tanks [22]. Zhong et al. designed a gliding robotic fish based on an underactuated flexible propulsion mechanism, which

* Corresponding author.

E-mail address: zhongyong@scut.edu.cn (Y. Zhong).

achieves two modes of motion: swimming and gliding [23]. Zheng et al. conceived the design of an active tail-driven robotic fish, incorporating a center of gravity adjustment mechanism [24]. They also developed a three-dimensional dynamic model. Current research on bionic robotic fish has achieved efficient bionic propulsion through various types of drive mechanisms, but still suffers from insufficient maneuverability and slow response in three-dimensional motion space.

Significant progress in bionic design, intelligent control, and underwater sensing capabilities of robotic fish through existing research has opened new frontiers in enhanced maneuverability and practical adaptability. Recent advancements in the field of hybrid propulsion architectures, encompassing the coordination of multiple propulsion mechanisms, have emerged. The integration of a hybrid drive system with traditional vector propulsion has emerged as a promising approach to enhance the locomotive capabilities of bionic robotic fish. Ji et al. proposed a bionic robotic fish that combines tail fin and rear propeller propulsion to easily execute a multi-modal swimming gait [25]. The research focused more on three-dimensional path tracking in hybrid drive modes. Tang et al. developed an underwater gliding snake robot that integrates a glider with an underwater snake robot [26]. Li et al. developed a miniature robotic fish equipped with double fixed propellers, with the ability to move in three dimensions in a narrow space [27,28]. However, the dynamics model constructed does not require consideration of the coupling because the propellers do not interfere with the propulsion of the caudal fins. In comparison with the single propulsion mode, the hybrid propulsion mode, which integrates the conventional thruster with the bionic propulsion mechanism, has demonstrated significant research potential in the domains of attitude control, path tracking, and motion performance enhancement of the robotic fish.

The central objective of this paper is to propose a hybrid drive bionic robotic fish based on pectoral-fin propeller propulsion and caudal-fin propulsion, and to construct the dynamic models of the robotic fish under a hybrid propulsion system with coupling. Secondly, a dynamic model of a hybrid drive bionic robotic fish was constructed based on the Newton–Euler method. The model was developed in conjunction with a hydrodynamic calculation method for the caudal fin that takes into account the influence of the propeller wake current. Finally, the hydrodynamic parameters were determined through computational fluid dynamics (CFD) simulation and optimization equations. The accuracy of the kinetic model in predicting velocity and trajectory was verified through kinematic experiments and simulations, including straight swimming motion, steering motion, and three-dimensional (3-D) spiral motion.

2. Materials and methods

2.1. Mechatronics design of the robotic fish

As illustrated in Fig. 1, the propulsion system of the designed hybrid drive bionic robotic fish consists of a pair of pectoral fin propellers and a caudal fin driven by a servo. The caudal fin drive part adopts the BCF mode. The single-jointed caudal fin is driven by the servo to carry out oscillatory motion, thereby generating the thrust required for the fish to move forward. This configuration ensures a propulsive effect while maintaining a compact overall structure. The pectoral fin propellers are symmetrically mounted on the robotic fish, and the internal pectoral fin servo changes the propelling direction of the propellers, enabling the robotic fish to exhibit 3-D spatial movement capability. The head of the robotic fish is sealed by waterproof grooves and silicone gaskets, and the dynamic sealing effect of the pectoral fin drive shaft is achieved by installing Glyd-ring in the pectoral fin drive hole.

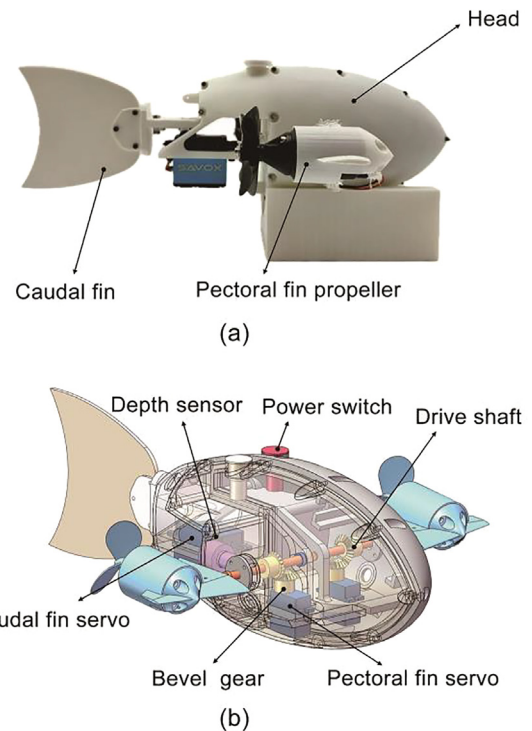


Fig. 1. Overview of the robotic fish. (a) Prototype. (b) Conceptual design.

Table 1
Specifications of the robotic fish.

Item	Characteristics
Dimension (L×W×H)	31 cm × 24 cm × 9.5 cm
Total mass	1.13 kg
Power supply	7.4 VDC, 1300 mAh Ni-H battery
Propeller nominal voltage	12 V
Microcontroller	STM32F103C8T6
Inertial measurement unit	MPU6050
Communication module	E62-433T20D

Furthermore, the robot fish is equipped with multiple sensors. A depth sensor is positioned at the anterior of the robotic fish, meticulously monitoring the dive depth. An inertial measurement unit (IMU) is integrated within the robotic fish, enabling precise monitoring of the six-axis acceleration. Concurrently, a power monitoring module has been integrated into the drive circuit of the fish, thereby enabling the monitoring of power consumption. The design specifications of the bionic robotic fish are delineated in Table 1.

2.2. Motion control

Bio-inspired control is employed to achieve autonomous robotic locomotion by emulating the rhythm generation mechanism of the animal central nervous system using a central pattern generator (CPG). The CPG generates stable periodic signals based on mutual inhibition among neurons without external inputs or high-level neural interventions, and this mechanism aligns with the spinal cord locomotion coordination mechanism of fishes. In this study, we have made improvements to Ijspeert's salamander-like CPG model and simplified the multi-driver phase coupling for the single-joint caudal fin [29]. These modifications have enabled the successful driving of a bionic robotic fish, thereby realizing a

swimming gait reminiscent of a real fish. The CPG model used in this paper can be represented by the following equation:

$$\ddot{b} = k_b \left(\frac{k_b}{4} (B - b) - \dot{b} \right) \quad (1)$$

$$\ddot{m} = k_m \left(\frac{k_m}{4} (M - m) - \dot{m} \right) \quad (2)$$

$$\dot{\theta} = \omega \left[\frac{(1+R)^2}{4R} - \frac{R^2-1}{4R} \text{sign}(\sin(\theta)) \right] \quad (3)$$

$$\alpha = b + m \cos(\theta) \quad (4)$$

$$\text{sign}(\lambda) = \begin{cases} 1, \lambda > 0 \\ 0, \lambda = 0 \\ -1, \lambda < 0 \end{cases} \quad (5)$$

where M , ω , B , and R are the high-level control parameters of the CPG control model, correspond to the amplitude, angular velocity, offset, and the time ratio, respectively. These parameters enable the modulation of the motion of the robotic fish. M and ω represent the primary control parameters influencing the swimming velocity of the robotic fish, and their numerical values are positively associated with the observed swimming velocity. B primarily affects the steering capability of the robotic fish and signifies the zero-degree oscillation of the driver. θ represents the phase of the oscillator. m represent the amplitude of the model oscillator and gradually converges to M . b represent the offset value of the model oscillator and gradually converges to B . k_m and k_b are used for controlling the convergence speed, respectively. r denotes the ratio of time between the caudal fin oscillating from caudal median to both sides and recovering from both sides to the median. α donates the rotation angle of the caudal servo, which is the sole output quantity of the CPG model. More details and content can be found in the previous work of our subject group [30].

3. Dynamic model

3.1. Definition of the coordinate systems

In this study, in order to illustrate the motion state of the robotic fish more clearly, the global inertial coordinate system and the fish body coordinate system are defined, and the origin of the fish body coordinate system is assumed to coincide with the geometric center of the robotic fish. As shown in Fig. 2, $O_I - X_I Y_I Z_I$ denotes the global inertial coordinate system, and $O_f - X_f Y_f Z_f$ denotes the fish body coordinate system, and the definitions of the coordinate systems all follow the right-hand rule. The position of the robotic fish is denoted as $\mathbf{P}_I = [X_I, Y_I, Z_I]$. The velocity of robotic fish is denoted as $\mathbf{V}_I = \dot{\mathbf{P}}_I = [V_{Ix}, V_{Iy}, V_{Iz}]^T$ in $O_I - X_I Y_I Z_I$ and $\mathbf{V}_f = [V_{fx}, V_{fy}, V_{fz}]^T$ in $O_f - X_f Y_f Z_f$. The relationship between \mathbf{V}_I and \mathbf{V}_f can be expressed as

$$\mathbf{V}_I = T_V \cdot \mathbf{V}_f \quad (6)$$

where T_V represents the transformation matrix from $O_f - X_f Y_f Z_f$ to $O_I - X_I Y_I Z_I$.

$$T_V = \begin{bmatrix} \cos\theta \cos\psi & \sin\phi \sin\theta \cos\psi - \cos\phi \sin\psi & \cos\phi \sin\theta \cos\psi + \sin\phi \sin\psi \\ \cos\theta \sin\psi & \sin\phi \sin\theta \sin\psi + \cos\phi \cos\psi & \cos\phi \sin\theta \sin\psi - \sin\phi \cos\psi \\ -\sin\theta & \sin\phi \cos\theta & \cos\phi \cos\theta \end{bmatrix} \quad (7)$$

Similarly, $\boldsymbol{\omega}_I = [\dot{\phi}, \dot{\theta}, \dot{\psi}]^T$, $\boldsymbol{\omega}_f = [\omega_{fx}, \omega_{fy}, \omega_{fz}]^T$ are the angular velocities of the robotic fish under $O_I - X_I Y_I Z_I$ and $O_f - X_f Y_f Z_f$,

respectively, and the relationship between them can be expressed as

$$\boldsymbol{\omega}_I = T_\omega \cdot \boldsymbol{\omega}_f \quad (8)$$

where

$$T_\omega = \begin{bmatrix} 1 & \sin\phi \tan\theta & \cos\phi \tan\theta \\ 0 & \cos\phi & -\sin\phi \\ 0 & \sin\phi \sec\theta & \cos\phi \sec\theta \end{bmatrix} \quad (9)$$

ϕ , θ , ψ indicate the roll, pitch and yaw angles of the robotic fish respectively.

Based on approximate hydrodynamic calculations and the Newton–Euler equations, the equations of motion for the hybrid drive robotic fish moving in 3-D space can be expressed as

$$M(\mathbf{V}) \dot{\mathbf{V}} + C(\mathbf{V}) \mathbf{V} = \boldsymbol{\tau} \quad (10)$$

where $\mathbf{V} = [\mathbf{V}_f \boldsymbol{\omega}_f]^T$ is denoted as the velocity vector of robotic fish. $\boldsymbol{\tau}$ indicates the forces and moments exerted on the robotic fish. $M(\mathbf{V})$ denotes the mass matrix of the robotic fish rigid body with the inclusion of additional mass. $C(\mathbf{V})$ is the Coriolis and centripetal matrix of the robotic fish rigid body with the inclusion of additional mass.

3.2. 3-D force analysis

This section analyzes the forces and moments acting on the robotic fish. The designed hybrid drive robotic fish can move in three dimensions by changing the propulsion direction of the pectoral fin propeller. Since the forces acting on the robotic fish during motion are mainly from the horizontal and vertical planes, and the lateral forces acting on the robotic fish are small, we mainly analyze the force decomposition of the robotic fish in the $X_f - Y_f$ plane and the $X_f - Z_f$ plane.

As shown in Fig. 2(a), the lift $F_{Li}(i = 1, 2)$ and drag $F_{Di}(i = 1, 2)$ acting on the robotic fish's head are expressed as:

$$F_{Li} = \frac{1}{2} \rho |\mathbf{V}_{fi}|^2 A_i C_{Li} \beta_i \quad (11)$$

$$F_{Di} = \frac{1}{2} \rho |\mathbf{V}_{fi}|^2 A_i C_{Di} \quad (12)$$

where ρ is the density of the fluid, C_{Li} and C_{Di} are the lift and drag coefficients, respectively, and A_i is the wetted area of the head. \mathbf{V}_{fi} is the velocity vector sum of the robot fish in the plane, β_i is the attack angle of the robotic fish, defined as:

$$\beta_1 = \arctan(\mathbf{V}_{fy}, \mathbf{V}_{fx}) \quad (13)$$

$$\beta_2 = \arctan(\mathbf{V}_{fz}, \mathbf{V}_{fx}) \quad (14)$$

The robotic fish will rotate and oscillate periodically around the coordinate axis of the fish body during movement. The roll, pitch, and yaw moments of resistance that the robotic fish is subjected to during the process can be expressed as follows, respectively:

$$M_{Dj} = -C_{Mj} |\boldsymbol{\omega}_{ff}| \boldsymbol{\omega}_{ff} \quad (j = x, y, z) \quad (15)$$

where C_{Mj} are the drag moment coefficient. Since the designed hybrid drive bionic robotic fish carries two pectoral fin propellers that can be individually adjusted in the direction of propulsion, it is necessary to consider the lift F_{PL}^k and the drag F_{PD}^k ($k = 1, 2$) exerted on the pectoral fins, which are shown in Fig. 2(b) and can be expressed as follows:

$$F_{PL}^k = \frac{1}{2} \rho |\mathbf{V}_{f2}|^2 A_P^k C_{PL}^k \gamma_P^k \quad (16)$$

$$F_{PD}^k = \frac{1}{2} \rho |\mathbf{V}_{f2}|^2 A_P^k C_{PD}^k \quad (17)$$

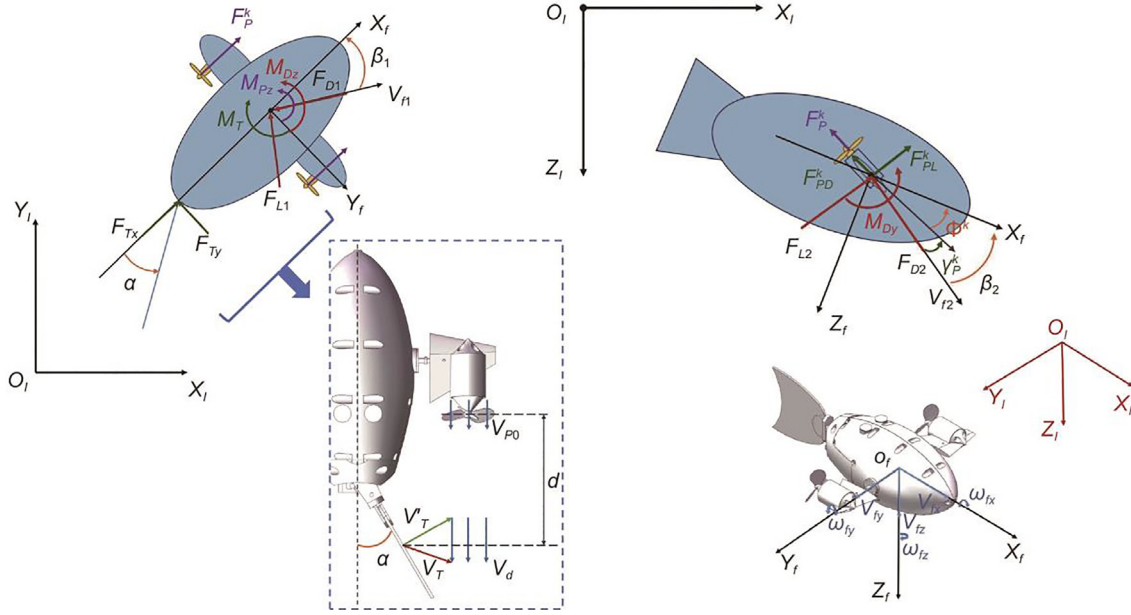


Fig. 2. Schematic diagram of the dynamic model of the robotic fish. (a) Force and velocity analysis for $X_f - Y_f$ plane. (b) Force and velocity analysis for $X_f - Z_f$ plane.

where F_{PL}^1 represents the lift applied to the left pectoral fin. F_{PD}^2 represents the drag applied to the right pectoral fin. A_p^k is the wetted area of the pectoral fin. γ_p^k denotes the attack angle of the pectoral fin, which is defined as $\gamma_p^k = \beta_2 - \Phi^k$. Φ^k is the propulsion angle of the pectoral fin propeller. C_{PL}^k, C_{PD}^k are the lift and drag hydrodynamic coefficients of the pectoral fins, respectively, and the magnitude of their values is related to the external dimensions of the pectoral fins and the attack angle.

According to the leaf element theory, the generalized force of the propeller can be expressed as [31]:

$$F_p^k = C_F \rho D^4 |n_i| n_i \quad (18)$$

$$T_p^k = C_T \rho D^5 |n_i| n_i \quad (19)$$

where F_p^k and T_p^k indicates force and torque, respectively. D represents the blade diameter of the propeller. n_i indicates the rotational speed of the propeller. C_F, C_T are the thrust coefficient and torque coefficient of the propeller, respectively, and are related to the propeller's own structure and the propulsion ratio J^k . The propulsion ratio J^k is calculated as follows:

$$J^k = \frac{U}{n_p^k D} \quad (20)$$

where U is the swimming speed of the robotic fish.

The Morison equation provides a simplified expression for the hydrodynamic force generated by caudal fin oscillation, which encompasses drag and additional mass forces. As shown in Fig. 2(a), in the hybrid propulsion mode, the wake generated by the pectoral fin propellers will interfere with the swing of the caudal fin, thereby affecting its propulsion effect. To simplify the model, the interference is considered only when the propeller jet angle, denoted by Φ^k , is set to zero. In the analysis of the velocity characteristics of the propeller wake, the jet of the propeller is regarded as a constant fluid, and the axial velocity of the propeller is identified as the primary index for consideration. The initial outflow velocity V_{p0} of the fluid at the paddle surface, subsequent to acceleration by the propeller, can be expressed as follows [32]:

$$\mathbf{V}_{p0} = 1.22 n_p^{k,1.01} D^{0.84} C_F \quad (21)$$

The jet region of the propeller can be divided into the flow establishment zone (ZFE) where the jet is formed and established,

and the established flow zone (ZEF) where the jet is attenuated, and the lengths of the zones are $0 < d/D \leq 3.15$,

$3.15 < d/D$ [33]. In this design, the caudal oscillation region is located in the flow establishment zone (ZFE), where the maximum axial velocity of the fluid can be expressed as [34]

$$\mathbf{V}_d = \left(1.51 - 0.175 \left(\frac{d}{D} \right) - 0.46P \right) \mathbf{V}_{p0} \quad (22)$$

where d is the jet distance. P is the propeller pitch, which is the ratio of propeller pitch to diameter.

Therefore, the Morison equation considering the propeller wake velocity \mathbf{V}_d located in the caudal swing region can be expressed as follows:

$$f(n) = -\frac{1}{2} \rho C_d \mathbf{V}_T |\mathbf{V}_T| b(n) - \rho C_m \dot{\mathbf{V}}_T s(n) \quad (23)$$

$$\mathbf{F}_T = \begin{bmatrix} F_{Tx} \\ F_{Ty} \end{bmatrix} = \int_0^{L_T} f(n) dn \quad (24)$$

$$M_T = \int_0^{L_T} r_n \times f(n) dn \quad (25)$$

where C_d and C_m are the drag coefficient and inertia coefficient, respectively. $b(n), s(n)$ denote the chord length and the caudal interface area at any point n of the caudal fin, respectively. r_n represents the position vector from point n to the center of the fish's mass. $\mathbf{V}_T = \mathbf{V}'_T + \mathbf{V}_d$ denotes the combined velocity vector of the fluid plasmas on the surface of any point n of the caudal fin. \mathbf{V}'_T represents the velocity vector generated by the caudal alone in still water driven by the servo. L denotes the distance from the caudal fin of the robotic fish to the center of mass.

4. Simulations and experiments

In order to verify the accuracy of the proposed hybrid drive bionic robotic fish dynamics model, extensive simulations and experiments are conducted in this section. Initially, the hydrodynamic coefficients of the robotic fish are calculated by computational fluid dynamics (CFD). In the subsequent stage of the research, the experimental measurements are compared with the simulation data in order to verify the accuracy of the proposed model under three distinct motion scenarios (namely, straight

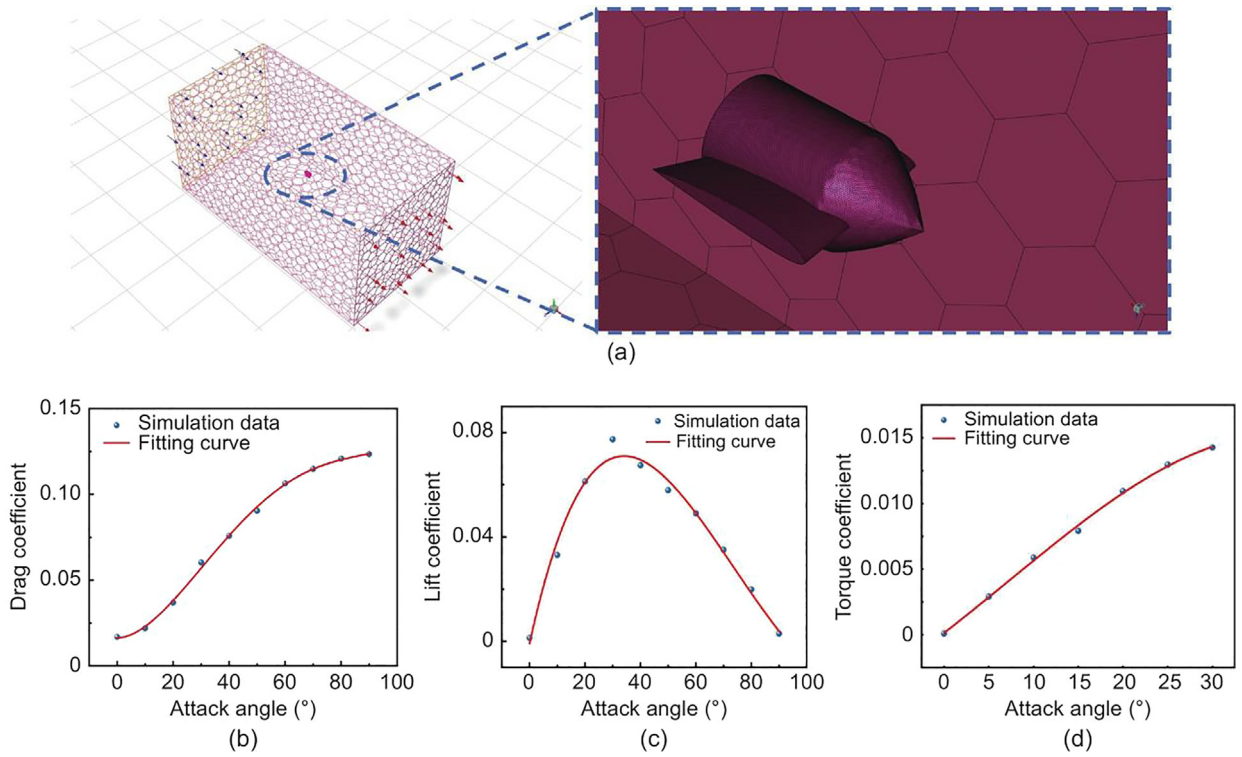


Fig. 3. Schematic of CFD fluid simulation. (a) Fluid field settings. (b) Simulation results of drag moment coefficient. (c) Simulation results of pectoral fin lift coefficient. (d) Simulation results of pectoral fin drag coefficient.

swimming, steering, and 3-D spiral dive, respectively). The measures of the swimming velocity, turning diameter, and motion trajectory of the robotic fish are the focus of this comparison.

4.1. Determination of hydrodynamic coefficients

For enhancing the precision of the hybrid drive bionic robotic fish dynamics model, the hydrodynamic coefficients of the robotic fish and pectoral fins were fitted at varying tack angles. In order to accomplish this objective, the CFD method was employed in order to calculate the hydrodynamic coefficients of the robotic fish and pectoral fins. Furthermore, the equations of the hydrodynamic coefficients versus the attack angle were also calculated. The drag moment coefficients of the robotic fish along the z-axis of the fish coordinate system and the lift and drag coefficients of the pectoral fins were the primary focus of the present analysis. Fig. 3(a) shows the meshing and fluid domain in the CFD simulation environment. The size of the fluid domain is 1000 mm × 1500 mm × 1000 mm and the model is placed in the center of the fluid domain. Given that the size of the simulation model is considerably smaller than that of the fluid domain, the fluid domain can be regarded as an infinite domain. The minimum mesh size of the solved model is 1 mm, the maximum mesh size of the fluid domain is 20 mm, and the number of boundary layers is 10. The hydrodynamic coefficients of the robotic fish pectoral fins are solved for different attack angles, and the results are shown in Fig. 3(b)(c)(d).

Given the modest range of yaw angle variation exhibited by the robotic fish in its natural movement, the yaw angle range of the model, designated as the lift coefficient, was set to [0°, 30°] in the CFD analyses. Similarly, the range of the pectoral fin's jet angle was set to [0°, 90°]. The observed increase and subsequent decrease in the lift coefficient of the pectoral fin in Fig. 3(c) is attributed to the occurrence of the stall phenomenon when the attack angle exceeds a critical value. This results in the separation

Table 2

Physical parameters of robotic fish.

Parameter meaning	Parameter	Values
Robotic Fish Weight	m_f	1.13 kg
x-axis additional mass	m_x	0.5424 kg
y-axis additional mass	m_y	1.017 kg
z-axis additional mass	m_z	1.017 kg
Caudal fin length	L_T	0.1 m
Caudal fin width	L_w	0.095 m
Fluid density	ρ	1000 kg/m ³
x- moment of inertia	I_x	1.278×10^{-3} kg/m ²
y- moment of inertia	I_y	2.928×10^{-3} kg/m ²
z- moment of inertia	I_z	2.981×10^{-3} kg/m ²
Wetted area of robotic fish	A_i	5.791×10^{-2} m ²
Wetted area of pectoral fin	A_p^k	1.239×10^{-2} m ²

of the boundary layer of the fluid flowing over the upper surface of the pectoral fin due to the backpressure gradient and viscous effects. Consequently, as the attack angle increases, the lift on the pectoral fin decreases. The equations for the hydrodynamic coefficients were fitted according to the CFD simulation results as follows:

$$C_{PD}^k = 4.3595 \times 10^{-9} \gamma_p^{k4} - 1.0261 \times 10^{-7} \gamma_p^{k3} + 6.9452 \times 10^{-5} \gamma_p^{k2} + 7.7335 \times 10^{-5} \gamma_p^k + 0.01631 \quad (26)$$

$$C_{PL}^k = -1.2984 \times 10^{-9} \gamma_p^{k4} + 6.5471 \times 10^{-7} \gamma_p^{k3} - 1.01993 \times 10^{-4} \gamma_p^{k2} + 0.0048 \gamma_p^k + 0.00447 \quad (27)$$

$$C_{Mz} = -2.12 \times 10^{-7} \beta_1^3 + 4.58 \times 10^{-6} \beta_1^2 + 5.25 \times 10^{-4} \beta_1 + 1.51 \times 10^{-4} \quad (28)$$

In addition to this, the remaining hydrodynamic coefficients in the kinetic model are determined by the following optimization

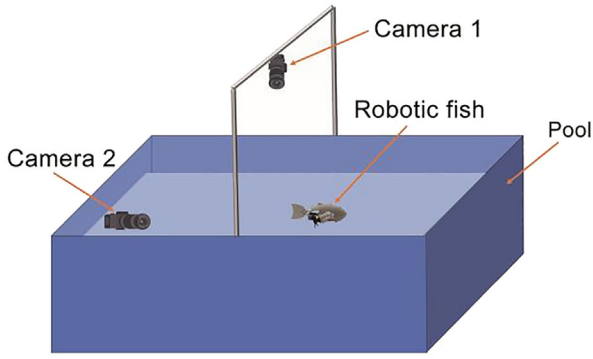


Fig. 4. Swimming experiment setting.

equations:

$$\min_{\lambda} \frac{1}{N} \sum_{n=1}^N \frac{1}{(N_e - N_s) T} \int_{N_s T}^{N_e T} |V_{ef,n}(t) - V_{sf,n}(t)| dt$$

$$s.t. \lambda_l \leq \lambda \leq \lambda_u \quad (29)$$

where $V_{ef,i}(t)$ and $V_{sf,i}(t)$ are the experimental and simulation velocity of the robotic fish for parameter set n . N denotes the number of parameter groups. T is the caudal oscillation period, λ is the set of hydrodynamic coefficients including C_{Li} , C_{Di} , C_d , C_m . λ_l and λ_u are the lower and upper limits of λ .

The physical parameters of the robotic fish used for parameter recognition and CFD simulation are given in Table 2. The finalized hydrodynamic coefficients in the kinetic model are $C_{L1} = 10$, $C_{L2} = 0.05$, $C_{D1} = 0.2$, $C_{D1} = 0.05$, $C_d = 1$, $C_m = 1$.

4.2. Experimental setup

As shown in Fig. 4, the straight swimming and steering experiments of the robotic fish are conducted in a pool measuring 4 m in length, 3 m in width, and 0.5 m in depth. A global camera (Camera 1) with a resolution of 1920×1080 pixels and a frame rate of 60 frames per second is mounted at the top of the pool to record the movement of the robotic fish in the $X_l - Y_l$ plane. The 3-D experiment was conducted in a 3 m long, 2 m wide, 1.5 m deep pool, in which a waterproof and anti-shaking motion camera (Camera 2) capable of shooting 4K resolution, 60 Hz video was placed beneath the surface of the pool and used to record the motion of the robotic fish underwater. The position and velocity of the robotic fish during its movement were calculated by capturing the marker points on the robotic fish through software. The adjustment of the buoyancy of the robotic fish was such that 90% of its body was submerged in water. The movement of the robotic fish was controlled remotely via the transmission of advanced motion parameters from the CPG and the jet angle ϕ^k and rotational speed n_p^k of the pectoral fin propeller through the computer.

4.3. Straight swimming motion

In this section, multiple control experiments were set up based on the characteristics of hybrid propulsion with a pectoral fin propeller with a jet angle of $\phi^k = 0^\circ (k = 1, 2)$. The rotational velocity n_p^k was set to 0 rpm, 300 rpm and 600 rpm, respectively. The advanced kinematic parameters of the CPG were transmitted through the host computer, where the pendulum amplitude $M = 10^\circ \sim 30^\circ$, the frequency $f = 0.5 \text{ Hz} \sim 2 \text{ Hz}$, the bias $B = 0^\circ$, and the time ratio $R = 1$.

These parameters were analyzed to determine the velocity of the hybrid propulsion bionic robotic fish's straight-swimming motion in a two-dimensional plane. The average swimming velocity between multiple sets of experiments and simulations were compared as shown in Fig. 5.

The results show that the simulation results of the proposed kinetic model fit well with the experiments, with a maximum error of 15.95% and an average error of 4.83% in the mean velocity. Additionally, the experimental findings demonstrate that the robotic fish's propulsion velocity in the hybrid propulsion mode is notably higher than in the caudal-only mode. With constant frequency and amplitude of caudal swing, the maximum velocity gain achieved at $n_p^k = 300 \text{ rpm}$ was 8.27, the average velocity gain was 1.87, and the maximum swimming velocity was 0.24 m/s (0.77 BL/s, Body length per second). Similarly, at $n_p^k = 600 \text{ rpm}$, the maximum velocity gain was 14.54, the average velocity gain was 3.59, and the maximum swimming velocity was 0.34 m/s (1.10 BL/s). In addition, the ultimate swimming velocity of the robotic fish is up to 0.79 m/s (2.54 BL/s).

Furthermore, the hybrid propulsion caudal hydrodynamic modeling was validated by comparing the velocity characteristics of the robotic fish in hybrid propulsion mode under different swing amplitudes. As illustrated in Fig. 6, the straight swimming speeds of the robotic fish under different swing amplitudes were compared at $n_p^k = 600 \text{ rpm}$ and $f = 1.5 \text{ Hz}$. The simulation results indicate that, in the absence of consideration for the coupling between the pectoral fin propeller and the caudal fin in the kinetic model, the simulated swimming velocity of the robotic fish exhibits significant fluctuations with increasing swing amplitude. Conversely, the experimental results demonstrate that the swimming velocity of the robotic fish exhibits less variability with increasing caudal fin swing amplitude and does not exhibit substantial fluctuations. This experimental phenomenon is also evident in the results of the other groups, and the kinetic model that takes the coupled situation into consideration likewise reflects this phenomenon. This is due to the presence of the propeller wake, which interferes with the swing of the caudal fin, resulting in the main factor affecting the swimming speed of the robotic fish being the rotational speed of the propeller rather than the swing of the caudal fin.

4.4. Steering motion

The accuracy of the robotic fish model is primarily validated through a comparison of the turning diameters of the robotic fish in the experiment and the simulation. In this experiment, the rotational velocity of one side propeller $n_p^1 = 0, 300$ and 600 rpm , while the other side n_p^2 was kept at zero. The CPG parameters were set to the pendulum amplitude $M = 10^\circ \sim 20^\circ$, bias B was set to 15° , and 20° , frequency f was set to 0.5 Hz , and 2 Hz , and time ratio $R = 1$, respectively. Additionally, the jet angle of the pectoral fin propeller was maintained at the same level as that of the straight swimming experiment.

As demonstrated in Fig. 7, the simulation outcomes derived from the dynamics-based model exhibit a strong correlation with the experimental results. Specifically, the mean absolute error (MAE) in the turning diameter is 0.0549 m, and the mean percentage of error is 11.21% when comparing the turning diameter at the propeller velocity $n_p^k = 0 \text{ rpm}$. At velocity $n_p^k = 300 \text{ rpm}$, the MAE is 0.0235 m with an average percentage error of 5.694%; at speed $n_p^k = 600 \text{ rpm}$, the MAE is 0.0114 m with an average percentage error of 2.39%. From the results, it can be seen that the hybrid propulsion mode can give the robotic fish a smaller turning diameter during the steering process, and its turning diameter becomes smaller as the propeller velocity increases. Meanwhile, the propeller mainly provides the forward speed of

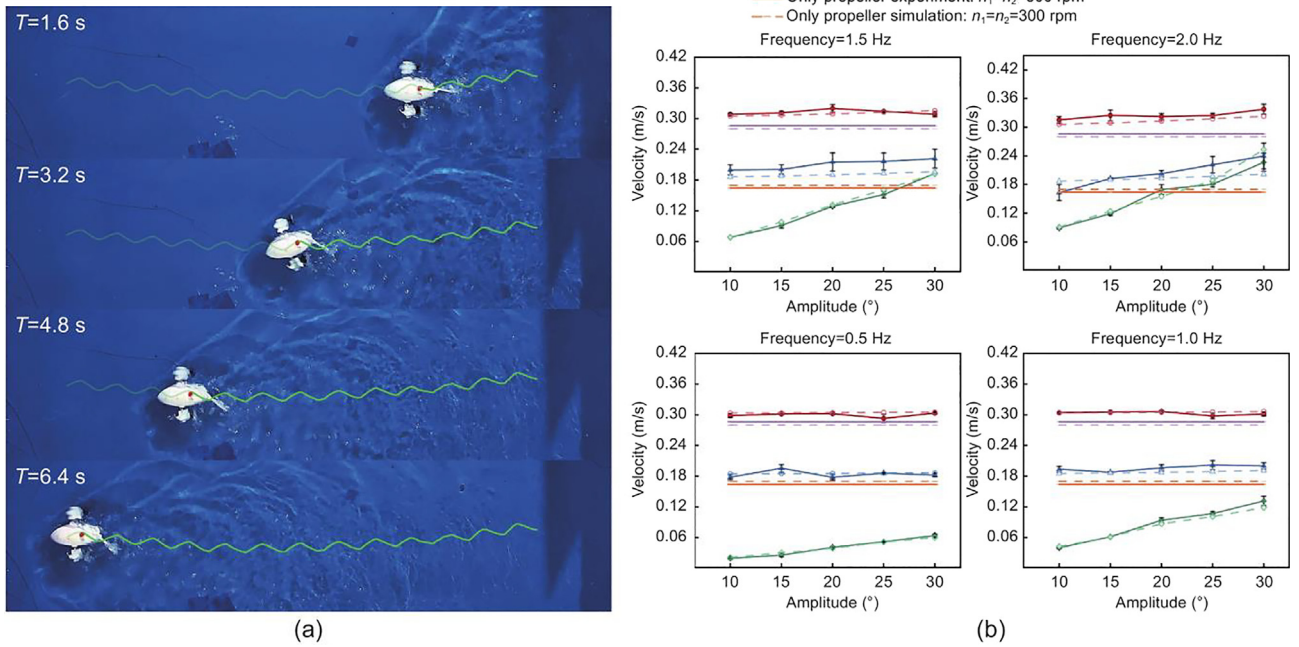


Fig. 5. Experimental and simulation results of straight swimming motion of robotic fish. (a) The swimming process of the robotic fish: $M = 20^\circ$, $B = 0^\circ$, $f = 2$ Hz, $R = 1$, $n_1 = n_2 = 600$ rpm. Average velocity at frequency (b) $f = 0.5$ Hz, (c) $f = 1$ Hz, (d) $f = 1.5$ Hz, and (e) $f = 2$ Hz.

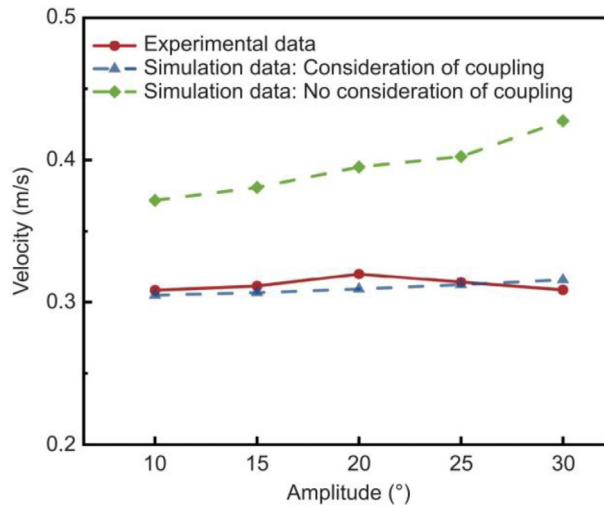


Fig. 6. Comparison of straight swimming velocity.

the robotic fish, while the caudal acts as a rudder to influence the angular velocity of the robotic fish, which increases significantly with the increase of bias B as shown in Fig. 8. In addition, the ultimate angular velocity of the robotic fish was experimentally measured to be 2.77 rad/s.

4.5. 3-D spiral dive motion

By adjusting the pitch angle of the pectoral fin propeller, the designed robotic fish can perform three-dimensional space movements, such as rapid up-and-down diving and spiral diving. In this section, the validity of the dynamics model is mainly verified by comparing the trajectories of the robotic fish in the spiral dive motion. In this section, the pectoral fin propeller has a pitch angle of $\phi^k = 50^\circ$ and a rotational velocity of $n_p^k = 540$ rpm, which

generates forward thrust, at which time the propeller wake does not interfere with the oscillation of the caudal fin. The advanced control parameters of the CPG are $M = 20^\circ$, $B = 20^\circ$, $f = 1$ Hz, and $R = 1$. The 3D experimental motion trajectory of the robotic fish was obtained by overlaying the data captured by two cameras, Camera 1 record the $X_l - Y_l$ plane motion of the robotic fish, and Camera 2 record the diving motion of the robotic fish.

The experimental results are shown in Fig. 9. Both experimental and simulated data are subjected to data processing by the Savitzky-Golay filter. The trajectory of the simulation based on the dynamical model can better track the experimentally measured trajectory. The mean square error (MSE) of its position coordinates is 0.006 m, the root mean square error (RMSE) is 0.078 m, and the maximum position error is 0.033 m. In the spiral dive, the force in the depth direction is mainly provided by

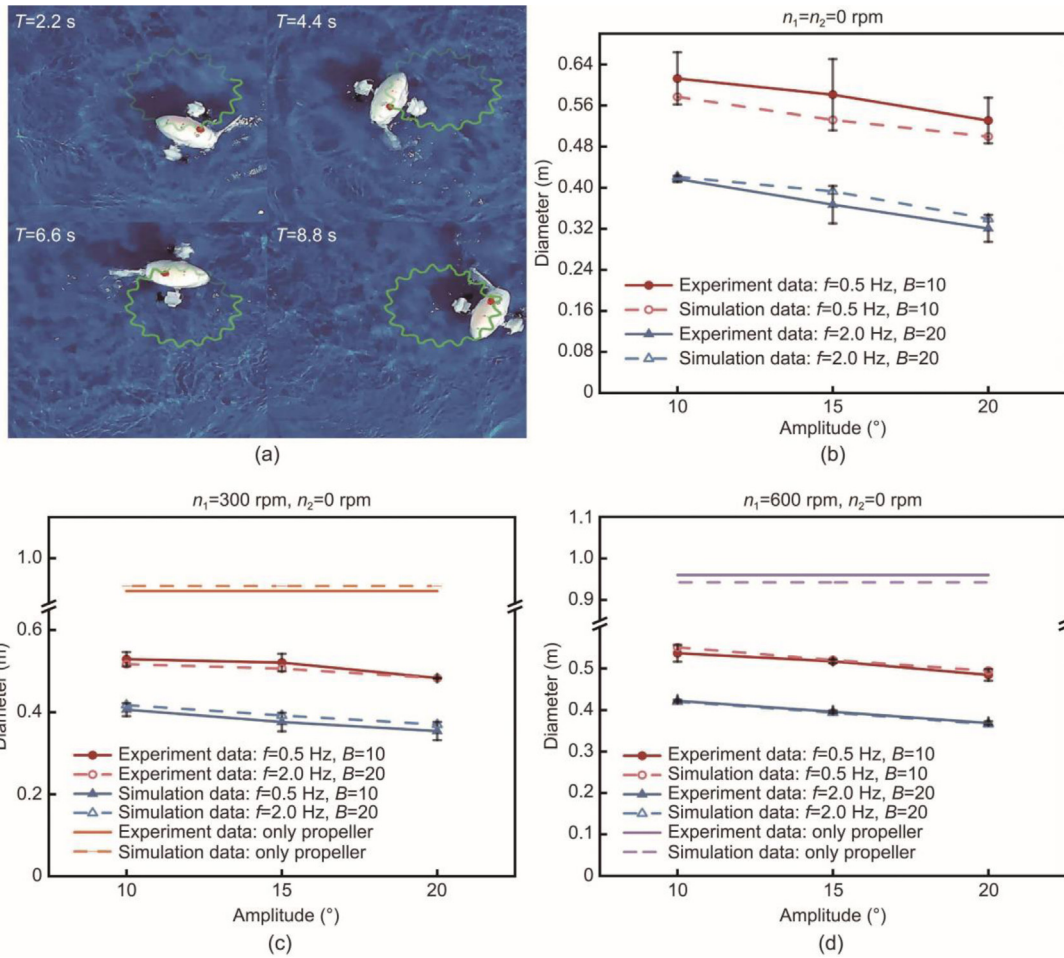


Fig. 7. Experimental and simulation results of steering motion of robotic fish. (a) The swimming process of the robotic fish: $M = 20^\circ$, $B = 20^\circ$, $R = 1$, $n_1 = 300$ rpm, $n_2 = 0$ rpm. Turning diameter at (b) $n_1 = n_2 = 0$ rpm, (c) $n_1 = 300$ rpm, $n_2 = 0$ rpm, and (d) $n_1 = 600$ rpm, $n_2 = 0$ rpm.

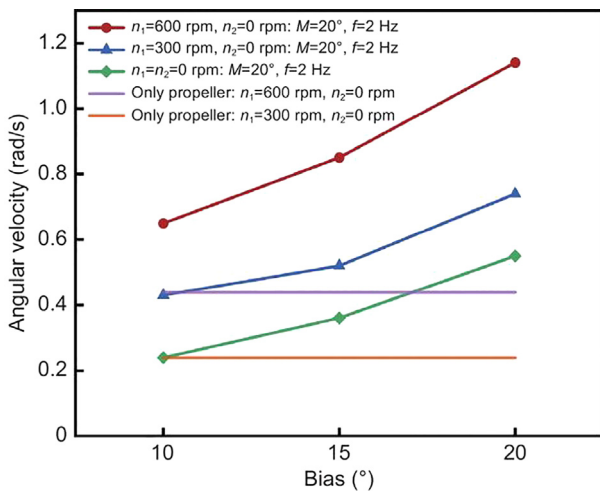


Fig. 8. Comparison of steering angular velocity of robotic fish.

the propeller, and the diving velocity depends on the rotational velocity of the propeller. The tail provides the moment for the robotic fish to steer, and the size of the steering radius depends on the input CPG parameters.

5. Conclusion

Researchers have been committed to developing a robotic fish whose locomotor performance can be comparable to that of real fish. However, at this stage, the locomotor ability of the bionic robotic fish has not yet met the demand, resulting in the inability to further promote its application to real production practice. In this work, we designed a hybrid propulsion system based on pectoral fin propeller and caudal fin propulsion, and utilized the pectoral fin servo to adjust the propeller's propulsion direction to construct a hybrid drive bionic robotic fish with three-dimensional locomotor capability. Simulation and experimental results show that the robotic fish combines the features of bionic propulsion and propeller propulsion. In terms of locomotion performance, the pectoral fin propeller significantly improves the straight-line swimming velocity of the robotic fish, while the bionic caudal oscillation mechanism effectively enhances the maneuvering performance, which can generate a high instantaneous angular acceleration. The experimental results show that the robotic fish in the hybrid drive mode has better steering characteristics, which are manifested in a smaller turning radius and higher steering angular velocity. Compared with the traditional bionic pectoral fin drive and internal buoyancy control system, the hybrid drive system proposed in this study achieves a wider range of deep thrust output by precisely controlling the propeller drive direction and speed. This innovative design significantly improves the three-dimensional spatial motion control capability of robotic fish, providing reliable technical support for them to

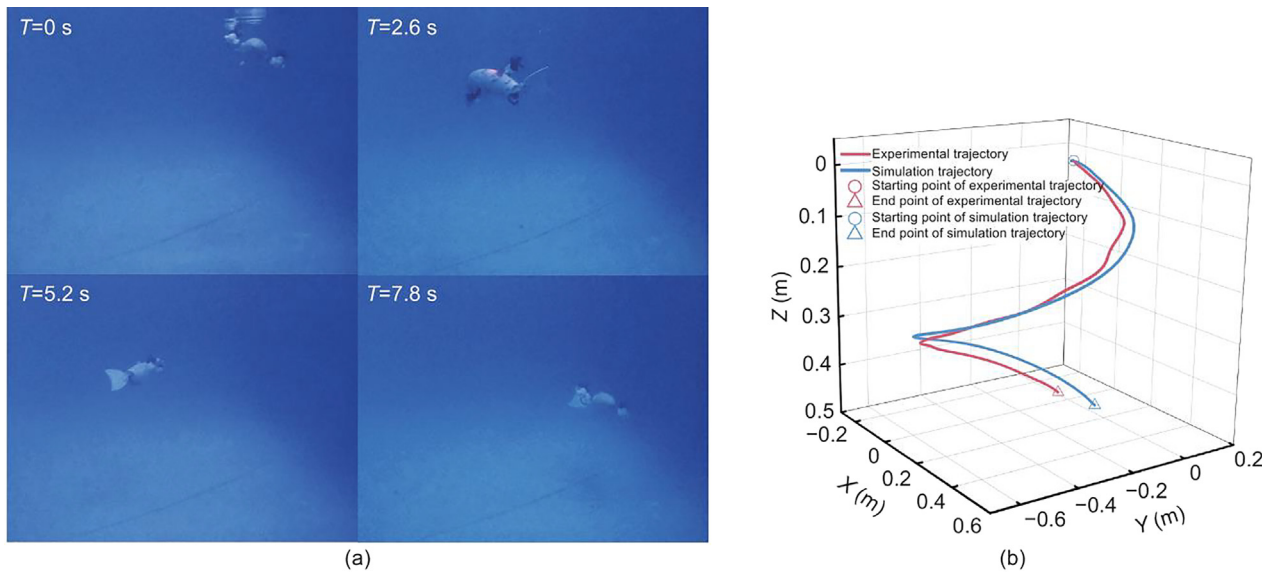


Fig. 9. Experimental and simulation results of robotic fish motion trajectories. (a) The swimming process of the robotic fish. (b) Comparison of simulated and experimental trajectories.

perform complex underwater operation tasks. Since the contour interface of the designed robotic fish is approximately circular, the effect of structural asymmetry is ignored in the dynamics calculations. Simplifications of the coincident geometric center of mass and axisymmetric body profile may introduce errors in kinetic model predictions in the presence of asymmetric mass distributions or imperfect structures. Further analysis is essential to strengthen the model to cope with real-world perturbations.

This paper sets forth a hybrid drive bionic robotic fish architecture that synergistically integrates pectoral-fin-mounted propellers with a caudal-fin-based propulsion system. A three-dimensional dynamic model is established using the Newton-Euler method to characterize the coupled interactions between the dual propulsion modes. This incorporates a hydrodynamic framework that accounts for the influence of propeller wake effects on caudal fin performance. The hydrodynamic parameters, including drag and lift coefficients, are determined through CFD simulations and optimization equations. The experimental validation process has demonstrated the model's accuracy in predicting key locomotion metrics. These include cruising velocity, turning radius and three-dimensional trajectory. The results reveal that the hybrid propulsion mode significantly enhances swimming performance compared to single-mode propulsion. Specifically, the robotic fish achieves a maximum velocity of 0.79 m/s (2.54 BL/s) in hybrid mode, with turning radii reduced by up to 11.21% under propeller-assisted steering. The adjustable pectoral-fin propellers enable versatile 3-D maneuvers, including spiral diving and rapid depth transitions, by modulating thrust direction. Furthermore, the model's fidelity is confirmed through quantitative comparisons, with an average velocity prediction error of 4.83% and a trajectory root mean square error (RMSE) of 0.078 m.

Future work will focus on advanced motion control strategies for 3-D spatial navigation and optimization of propulsion efficiency in redundant drive configurations. Additionally, integrating adaptive algorithms to mitigate wake interference and exploring energy-efficient gaits under hybrid propulsion will further enhance the robotic fish's operational capabilities in complex underwater environments.

CRediT authorship contribution statement

Haoyu Huang: Writing – review & editing, Writing – original draft, Methodology, Investigation, Formal analysis. **Shuai Xian:** Software, Resources, Project administration, Formal analysis, Data curation. **Chengye Xiong:** Supervision, Resources, Project administration, Data curation, Conceptualization. **Weihua Li:** Visualization, Validation, Supervision, Project administration, Methodology. **Yong Zhong:** Visualization, Validation, Supervision, Project administration, Methodology, Investigation, Conceptualization.

Declaration of competing interest

The authors declare that they have no known competing financial interests or personal relationships that could have appeared to influence the work reported in this paper.

Acknowledgments

This work was supported in part by the National Natural Science Foundation of China (62473161), the Natural Science Foundation of Guangdong Province (2024A1515012582), Guangzhou applied Basic Research Project (2024A04J9942), and the GJYC program of Guangzhou (2024D03J0005).

Appendix A. Supplementary data

Supplementary material related to this article can be found online at <https://doi.org/10.1016/j.birob.2025.100247>.

References

- [1] A. Shukla, H. Karki, Application of robotics in offshore oil and gas industry—A review part II, *Robot. Auton. Syst.* 75 (2016) 508–524, <http://dx.doi.org/10.1016/j.robot.2015.09.013>.
- [2] M.K. Habib, Y. Baudoin, F. Nagata, Robotics for rescue and risky intervention, in: *IECON 2011-37th Annual Conference of the IEEE Industrial Electronics Society*, 2011, pp. 3305–3310.

- [3] S. Chutia, N.M. Kakoty, D. Deka, A review of underwater robotics, navigation, sensing techniques and applications, in: Presented at the Proceedings of the 2017 3rd International Conference on Advances in Robotics, New Delhi, India, 2017, <http://dx.doi.org/10.1145/3132446.3134872>.
- [4] A. Prakash, et al., Bioinspiration and biomimetics in marine robotics: a review on current applications and future trends, *Bioinspiration Biomimetics* 19 (3) (2024) 031002, <http://dx.doi.org/10.1088/1748-3190/ad3265>.
- [5] X. Wu, T. Sood, Z. Chen, J. Chen, Robotic fish enabled offshore pipeline inspection, in: Presented at the Offshore Technology Conference, 2023, <http://dx.doi.org/10.4043/32427-MS>.
- [6] M. Maslin, S. Louis, K. Godary Dejean, L. Lapiere, S. Villéger, T. Claverie, Underwater robots provide similar fish biodiversity assessments as divers on coral reefs 7 (4), 2021, pp. 567–578, <http://dx.doi.org/10.1002/rse2.209>.
- [7] R. Bogue, Underwater robots: a review of technologies and applications, *Ind. Robot.: An Int. J.* 42 (3) (2015) 186–191, <http://dx.doi.org/10.1108/IR-01-2015-0010>.
- [8] J. Li, W. Li, Q. Liu, B. Luo, W. Cui, Current status and technical challenges in the development of biomimetic robotic fish-type submersible, *OceanLand- Atmosphere Res.* 3, 0036, <http://dx.doi.org/10.34133/olar.0036>.
- [9] D. Romano, C. Stefanini, Any colour you like: fish interacting with bioinspired robots unravel mechanisms promoting mixed phenotype aggregations, *Bioinspiration Biomimetics* 17 (4) (2022) 045004, <http://dx.doi.org/10.1088/1748-3190/ac6848>.
- [10] Y. Zhong, L. Zheng, R. Du, Robot fish with two-DOF pectoral fins and a wire-driven caudal fin, *Adv. Robot.* 32 (1) (2018) 25–36, <http://dx.doi.org/10.1080/01691864.2017.1392344>.
- [11] B. Sun, et al., Recent progress in modeling and control of bio-inspired fish robots, *J. Mar. Sci. Eng.* 10 (6) <http://dx.doi.org/10.3390/jmse10060773>.
- [12] X. Zhou, K. Xia, H. Tu, H. Zhu, Y. Wei, F. Qu, Design and hydrodynamic analysis of a dual-drive bionic robotic fish, *Ocean Eng.* 319 (2025) 120234, <http://dx.doi.org/10.1016/j.oceaneng.2024.120234>.
- [13] G. Manduca, et al., A bioinspired control strategy ensures maneuverability and adaptability for dynamic environments in an underactuated robotic fish, *J. Intell. Robot. Syst.* 110 (2) (2024) 69, <http://dx.doi.org/10.1007/s10846-024-02080-9>.
- [14] Y. Zhong, Z. Hong, Y. Li, J. Yu, A general kinematic model of fish locomotion enables robot fish to master multiple swimming motions, *IEEE Trans. Robot.* 40 (2024) 750–763, <http://dx.doi.org/10.1109/TRO.2023.3339015>.
- [15] Q. Wang, Z. Hong, Y. Zhong, Learn to swim: Online motion control of an underactuated robotic eel based on deep reinforcement learning, *Biomim. Intell. Robot.* 2 (4) (2022) 100066, <http://dx.doi.org/10.1016/j.birob.2022.100066>.
- [16] Y. Zhong, Z. Li, R. Du, A novel robot fish with wire-driven active body and compliant tail, *IEEE/ASME Trans. Mechatronics* 22 (4) (2017) 1633–1643, <http://dx.doi.org/10.1109/TMECH.2017.2712820>.
- [17] Y. Liang, K. Wang, Y. Mo, Y. Zhong, A wire-driven flexible vector-propelled robotic fish with omnidirectional adaptive caudal fin, in: 2023 29th International Conference on Mechatronics and Machine Vision in Practice, M2VIP, 2023, pp. 1–6.
- [18] L. Cen, A. Erturk, Bio-inspired aquatic robotics by untethered piezohydroelastic actuation, *Bioinspiration Biomimetics* 8 (1) (2013) 016006, <http://dx.doi.org/10.1088/1748-3182/8/1/016006>.
- [19] A.D. Marchese, C.D. Onal, D. Rus, Autonomous soft robotic fish capable of escape maneuvers using fluidic elastomer actuators, *Soft Robot.* 1 (1) (2014) 75–87, <http://dx.doi.org/10.1089/soro.2013.0009>.
- [20] X. Chen, J. Yu, Z. Wu, Y. Meng, S. Kong, Toward a maneuverable miniature robotic fish equipped with a novel magnetic actuator system, *IEEE Trans. Syst. Man, Cybern.: Syst.* 50 (7) (2020) 2327–2337, <http://dx.doi.org/10.1109/TSMC.2018.2812903>.
- [21] S. Liu, C. Liu, G. Wei, L. Ren, L. Ren, Design, modeling, and optimization of hydraulically powered double-joint soft robotic fish, *IEEE Trans. Robot.* 41 (2025) 1211–1223, <http://dx.doi.org/10.1109/TRO.2025.3526087>.
- [22] Z. Chen, P. Hou, Z. Ye, Modeling of robotic fish propelled by a servo/IPMC hybrid tail, in: 2018 IEEE/RSJ International Conference on Intelligent Robots and Systems, IROS, 2018, pp. 8146–8151.
- [23] Y. Zhong, Q. Wang, J. Yang, C. Wang, Design, modeling, and experiment of underactuated flexible gliding robotic fish, *IEEE/ASME Trans. Mechatronics* 29 (3) (2024) 2266–2276, <http://dx.doi.org/10.1109/TMECH.2023.3328034>.
- [24] X. Zheng, M. Xiong, R. Tian, J. Zheng, M. Wang, G. Xie, Three-dimensional dynamic modeling and motion analysis of a fin-actuated robot, *IEEE/ASME Trans. Mechatronics* 27 (4) (2022) 1990–1997, <http://dx.doi.org/10.1109/TMECH.2022.3174173>.
- [25] Y. Ji, Y. Wei, J. Liu, D. An, Design and realization of a novel hybrid-drive robotic fish for aquaculture water quality monitoring, *J. Bionic Eng.* 20 (2) (2023) 543–557, <http://dx.doi.org/10.1007/s42235-022-00282-1>.
- [26] J. Tang, J. Chang, B. Li, A. Zhang, Modeling and control of hybrid-driven gliding motion for an underwater gliding snake-like robot, *Int. J. Control. Autom. Syst.* 19 (9) (2021) 3190–3198, <http://dx.doi.org/10.1007/s12555-020-0545-z>.
- [27] S. Li, Y. Li, Z. Wu, J. Wang, M. Tan, 3-D path following control for a miniature maneuverable robotic fish with hybrid actuators, in: 2022 IEEE International Conference on Real-Time Computing and Robotics, RCAR, 2022, pp. 7–12.
- [28] S. Li, Z. Wu, S. Dai, J. Wang, M. Tan, J. Yu, Tight-space maneuvering of a hybrid-driven robotic fish using backstepping-based adaptive control, *IEEE/ASME Trans. Mechatronics* 29 (5) (2024) 3219–3231, <http://dx.doi.org/10.1109/TMECH.2023.3338879>.
- [29] A.J. Ijspeert, A. Crespi, Online trajectory generation in an amphibious snake robot using a lamprey-like central pattern generator model, in: Proceedings 2007 IEEE International Conference on Robotics and Automation, 2007, pp. 262–268.
- [30] F. Xie, Y. Zhong, R. Du, Z. Li, Central pattern generator (CPG) control of a biomimetic robot fish for multimodal swimming, *J. Bionic Eng.* 16 (2) (2019) 222–234, <http://dx.doi.org/10.1007/s42235-019-0019-2>.
- [31] R. Izadi-Zamanabadi, M. Blanke, A ship propulsion system as a benchmark for fault-tolerant control, *Control Eng. Pract.* 7 (2) (1999) 227–239, [http://dx.doi.org/10.1016/S0967-0661\(98\)00149-X](http://dx.doi.org/10.1016/S0967-0661(98)00149-X).
- [32] G. Hamill, C. Kee, D. Ryan, Three-dimension efflux velocity characteristics of marine propeller jets, *Proc. Inst. Civ. Eng.: Marit. Eng.* 168 (2015) 62–75, <http://dx.doi.org/10.1680/maen.14.00019>.
- [33] M.L. Albertson, Y.B. Dai, R.A. Jensen, H. Rouse, Diffusion of submerged jets, *Trans. Am. Soc. Civ. Eng.* 115 (1) (1950) 639–664, <http://dx.doi.org/10.1061/TACEAT.0006302>.
- [34] G.A. Hamill, C. Kee, Predicting axial velocity profiles within a diffusing marine propeller jet, *Ocean Eng.* 124 (2016) 104–112, <http://dx.doi.org/10.1016/j.oceaneng.2016.07.061>.